Effect of bidirectional mechanoelectrical coupling on spontaneous oscillations and sensitivity in a model of hair cells

Rami M. Amro and Alexander B. Neiman*

Department of Physics and Astronomy, Ohio University, Athens, Ohio 45701, USA and Neuroscience Program, Ohio University, Athens, Ohio 45701, USA

(Received 22 September 2014; published 6 November 2014)

Sensory hair cells of amphibians exhibit spontaneous activity in their hair bundles and membrane potentials, reflecting two distinct active amplification mechanisms employed in these peripheral mechanosensors. We use a two-compartment model of the bullfrog's saccular hair cell to study how the interaction between its mechanical and electrical compartments affects the emergence of distinct dynamical regimes, and the role of this interaction in shaping the response of the hair cell to weak mechanical stimuli. The model employs a Hodgkin-Huxley-type system for the basolateral electrical compartment and a nonlinear hair bundle oscillator for the mechanical compartment, which are coupled bidirectionally. In the model, forward coupling is provided by the mechanoelectrical transduction current, flowing from the hair bundle to the cell soma. Backward coupling is due to reverse electromechanical transduction, whereby variations of the membrane potential affect adaptation processes in the hair bundle. We isolate oscillation regions in the parameter space of the model and show that bidirectional coupling affects significantly the dynamics of the cell. In particular, self-sustained oscillations of the hair bundles and membrane potential can result from bidirectional coupling, and the coherence of spontaneous oscillations can be maximized by tuning the coupling strength. Consistent with previous experimental work, the model demonstrates that dynamical regimes of the hair bundle change in response to variations in the conductances of basolateral ion channels. We show that sensitivity of the hair cell to weak mechanical stimuli can be maximized by varying coupling strength, and that stochasticity of the hair bundle compartment is a limiting factor of the sensitivity.

DOI: 10.1103/PhysRevE.90.052704 PACS number(s): 87.19.lt, 87.19.ln, 05.10.Gg, 05.45.Xt

I. INTRODUCTION

Sensory hair cells are mechanoreceptors transducing mechanical stimuli to electrical signals in auditory and vestibular periphery in vertebrates. The detecting element is located in the hair bundle, a ciliated structure on the apical side of the cell, which possesses mechanically gated ion channels: they open or close in response to deflection of the hair bundle. In this way deflection of the hair bundle is transferred to a flow of positively charged ions (mostly potassium) which depolarize the cell body. Exquisite sensitivity, frequency selectivity, and compressive nonlinearity are pronounced characteristics of sensory hair cells [1–4]. These characteristics are due to active processes in the machinery of both nonmammalian [5,6] and mammalian hair cells [7] (see Ref. [8] for a recent review). In particular, in some low-frequency nonmammalian hair cells, these active processes may result in spontaneous oscillations of the hair bundles [9], which enhances sensitivity and selectivity of the hair cell [10] and may result in collective phenomenon of otoacoustic emission [11,12].

Spontaneous hair bundle oscillations are inherently noisy due to several sources of randomness, which limits sensitivity and selectivity of the hair bundle to weak mechanical stimuli [13]. In bullfrog sacculus, free-standing hair bundles exhibit a diverse range of stochastic self-sustained oscillations, such as periodic, spiking, or bursting [9,14,15]. The frequency of these oscillations ranges from 5 to 50 Hz, and their amplitude can be as large as 80 nm [9]. Spontaneous hair bundle oscillations require two main processes to be in place [10]. First is the negative differential stiffness of the hair bundle stemming from the phenomenon of gating compliance of mechanoelectrical transduction (MET) channels [16] leading to mechanical instability of the hair bundle for small (few nm) displacements [17]. Second is the adaptation processes, which include active forces that are generated by calcium-controlled molecular motors, which shift the instability regions of negative stiffness [17–20]. Several studies suggested that the hair bundle may operate on the verge of Andronov-Hopf bifurcation, which provide the hair cell with giant sensitivity and sharp selectivity, along with the compressive nonlinearity [3,4,21,22]. Several models were developed to account for these observations [9,13,15,23–25], which reproduced well the details of spontaneous hair bundle oscillations and their dependence on parameters, e.g., concentration of calcium ions and a mechanical load.

Randomness of individual hair bundle oscillations can be reduced in a system of coupled cells, resulting in higher amplification and sharper response [26–28]. Furthermore, in the bullfrog sacculus, mechanical coupling of a hair bundle via an overlaying otolithic membrane suppresses spontaneous oscillations [29,30], and the amplification mechanism may be rooted in the phenomenon of amplitude death as suggested by a recent modeling study [31,32].

Variations of the membrane potential affect the hair bundle dynamics and the mechano-electrical transduction. Earlier studies documented the so-called reverse electromechanical transduction in which voltage and hair bundle fluctuations recorded simultaneously were correlated. Hair bundles deflect in response to somatic electrical stimulation [29,33]. Inhibition of basolateral potassium currents results in drastic changes in spontaneous dynamics of the hair bundle [34].

*neimana@ohio.edu

In low-frequency nonmammalian hair cells whereby Ca^{2+} ions controls slow adaptation process, the membrane potential variations are likely affect the driving force of Ca^{2+} and thus mediate the adaptation processes. We note, however, that a recent study showed that a mechanism of adaptation in high-frequency mammalian auditory hair cell is calcium independent [35].

Nonmammalian hair cells show oscillatory electrical responses and use electrical resonance as a tuning mechanism [36,37]. Furthermore, spontaneous self-sustained voltage oscillations were documented in saccular hair cells in frogs [38–40]. In particular, Rutherford and Roberts [40] documented diverse voltage oscillatory patterns in semi-intact preparation of bullfrog sacculus and correlated these patterns with the proportion of basolateral ionic currents. These oscillations were reflected in oscillatory excitatory postsynaptic potentials of afferent neurites and were able to trigger action potentials. The relatively large amplitude of the hair cell membrane potential oscillations (14–75 mV) [40] suggests that they may affect the hair bundle dynamics via reverse electromechanical transduction. In support, a recent study documented drastic changes of the hair bundle dynamics upon blockage of basolateral potassium ionic currents [34]. Nevertheless, the role of these electrical oscillations and bidirectional coupling in shaping the spontaneous and response dynamics of the hair cell are still unknown. Partially this is due to experimental difficulties in simultaneous recording of the hair bundle displacement and the membrane potential, which calls for a modeling approach. From the nonlinear dynamics perspective, the hair cell can be represented as two bidirectionally coupled nonlinear oscillators. First is the mechanical oscillator residing in the hair bundle, characterized by essential stochastic dynamics stemming from several noise sources [13]. Second is the electrical oscillator associated with the basolateral membrane, whose stochasticity is mainly due to noisy input via the MET ionic current from the hair bundle [41].

Previous efforts in modeling of nonmammalian hair cell dynamics were mostly devoted to either the hair bundle (cited above) or to the dynamics of the membrane potential [38,39,42–44]. A linear resonator model for the electrical oscillations coupled with the hair bundle dynamics was used in Ref. [45] to explain a possible mechanism of self-tuning of the hair cell to Andronov-Hopf bifurcation. A deterministic model of weakly coupled nonlinear mechanical and electrical compartments was studied in Ref. [46] showing that the electrical oscillator may enhance amplification and nonlinear compression in the vicinity of Andronov-Hopf bifurcation. A model of a linear electrical resonator coupled bidirectionally to stochastic hair bundle oscillator was used in Ref. [47] to predict that higher quality voltage oscillations may enhance coherence of mechanical hair bundle oscillations.

Here we develop a two-compartment model for bullfrog saccular hair cells, an experimental system which was studied in detail for decades in many experimental laboratories. The model is based on previously published data and modeling of mechanical and electrical compartments, it incorporates nonlinear dynamics of both the hair bundle and the membrane potential as well as forward mechanoelectrical and reverse electromechanical transduction mechanisms. We study deterministic and stochastic dynamics of the model as well as effects of bidirectional coupling on the sensitivity and selectivity of the cell to external mechanical stimuli. Some preliminary results were reported in a conference proceedings [48].

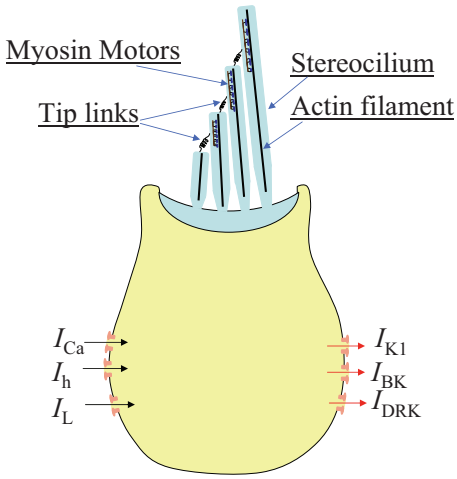

FIG. 1. (Color online) Schematic diagram of a hair cell highlighting the main components used in modeling. The hair bundle is composed of an array of stereocilia arranged in rows of increasing height. Neighboring stereocilia are linked by fine filaments, called the tip links. The hair bundle is immersed in potassium ion-rich endolymph, whereas the basolateral membrane of the hair cell is in contact with perilymph, characterized by a low potassium and a high sodium ion concentration. Mechanoelectrical transduction (MET) channels located on stereocilia open or close in response to deflection of the hair bundle, which stresses or relaxes the tip links. The myosin molecular motors anchored to the insertion plaque near MET channels contribute to adaptation. The basolateral membrane of the cell contains several types of ion channels, associated with specific ionic currents. Two sets of ionic currents are shown. First, inward currents include the voltage gated calcium current (I_{Ca}), mixed sodium and potassium h-type current (I_h), and leak current (I_L). Second, outward currents include the [Ca^{2+}]-regulated potassium BK current (I_{BK}) with its steady I_{BKS} and transient I_{BKT} components, delayed rectifier potassium current (I_{DRK}), and inwardly rectifier potassium current (I_{K1}).

II. MODEL AND METHODS

Figure 1 sketches a two-compartment model of the hair cell. We term these compartments mechanical, referring to the hair bundle, and electrical, corresponding to the cell soma or basolateral cell membrane. Both compartments are assumed to be at the same potential. A displacement of the hair bundle triggers opening or closing of mechanoelectrical transduction (MET) channels, resulting in variation of the MET current [49]. The MET current constitutes the forward, mechanical→electrical, coupling. Variation of the membrane potential may influence MET machinery in several ways. Ca^{2+} influx through MET channels changes in response to voltage variations, thus affecting various adaptation processes, e.g., the dynamics of myosin motors [18,50]. It may also affect tension in the intracellular element in series with tip link [33,51]. Furthermore, voltage variations may affect directly the dynamical state of MET channels [51]. Our

model assumes the first scenario, mentioned above, in which changes in $[Ca^{2+}]$ near molecular motors in response to voltage variations alter the force produced by these motors. This electromechanical transduction (EMT) [52] constitutes the backward, electrical→mechanical coupling in the model.

For the hair bundle (mechanical compartment) we adopted a model proposed in Ref. [13]. The hair bundle is treated as a single structure subjected to elastic forces, forces exerted by MET channels, forces exerted by myosin motors, and random forces. The overdamped motion of the hair bundle is described by two coupled Langevin equations (1): for the position of the hair bundle, X, and for the projection of the position of molecular motors on the horizontal axis, $X_a(t)$:

$$\begin{aligned}\lambda\frac{dX}{dt} &= -K_{\mathrm{GS}}(X - X_{\mathrm{a}} - DP_{\mathrm{o}}) - K_{\mathrm{SP}}X \\ &\quad + F_{\mathrm{ext}}(t) + \epsilon\sqrt{2k_{\mathrm{B}}T\lambda}\eta(t), \\ \lambda_{\mathrm{a}}\frac{dX_{\mathrm{a}}}{dt} &= K_{\mathrm{GS}}(X - X_{\mathrm{a}} - DP_{\mathrm{o}}) \\ &\quad - F_{\max}(1 - SP_{\mathrm{o}}) + \epsilon\sqrt{2k_{\mathrm{B}}T_a\lambda_{\mathrm{a}}}\eta_{\mathrm{a}}(t).\end{aligned} \tag{1}$$

Positive displacement of the hair bundle, $X > 0$, results in opening of MET channels and corresponds to deflection to the right in Fig. 1. Positive displacement of the molecular motors, $X_a > 0$, corresponds to the downward sliding of motors along the actin core. In the first equation of Eqs. (1), $F_{\mathrm{ext}}(t)$ stands for the external stimulus force, $K_{\mathrm{SP}} = 0.6$ mN/m is the combined stiffness of the stereocilia base and of the external mechanical load, $K_{\mathrm{GS}} = 0.75$ mN/m is the gating springs stiffness, $D = 60.9$ nm is the gating swing, i.e., the displacement generated by opening of the MET channel, and $\lambda = 2.8$ μNs/m and $\lambda_{\mathrm{a}} = 10.0$ μNs/m are the drag coefficients of the hair bundle and molecular motors, respectively. The open probability of MET channels, $P_{\mathrm{o}}(X, X_{\mathrm{a}})$, is given by

$$P_{\mathrm{o}}(X, X_{\mathrm{a}}) = \frac{1}{1 + A\, e^{-(X - X_{\mathrm{a}})K_{\mathrm{GS}}D/(Nk_{\mathrm{B}}T)}}, \tag{2}$$

with $A = e^{[\Delta G + K_{\mathrm{GS}}D^2/(2N)]/(k_{\mathrm{B}}T)}$, where $N = 50$ is the number of MET channels and $\Delta G = 10k_{\mathrm{B}}T$ is the free energy difference between closed and open state of the MET channel, $T = 300$ K is the temperature, and $T_a = 1.5T$ is an effective temperature of the motors. The second equation of Eqs. (1) describes adaptation dynamics: the first term refers to the so-called slipping adaptation, and the second term represents a Ca^{2+}-dependent climbing adaptation, i.e., the maximal force the motors can generate at given $[Ca^{2+}]$. Noise terms $\eta(t)$ and $\eta_{\mathrm{a}}(t)$ are two uncorrelated Gaussian white noise sources which represent the Brownian motion of the hair bundle in the viscous endolymph, cluttering of ion channels, and the stochastic binding and unbinding of molecular motors along actin filaments [13]. Dimensionless parameter ϵ takes two values: 0 for the deterministic case, and 1 for full noise strength. The control parameters of the hair bundle model are Ca^{2+}-feedback strength, S, and the maximal force generated by the motors when $[Ca^{2+}]$ vanishes, $F_{\max}$. Deterministic and stochastic dynamics of the hair bundle model was studied in details in Refs. [13,24,53,54].

Electrical compartment was modelled with a Hodgkin-Huxley-type system which was discussed in detail in Ref. [44]. It includes six ionic currents (Fig. 1) quantified in recent experimental studies of bullfrog saccular hair cells [38,40]. The inwardly rectifier potassium current I_{K1} (K1) has steady state half activation potential $V_{1/2} = -110$ mV and reversal potential $E_k = -95$ mV and deactivates for potentials positive to $V_0 = -55$ mV. The so-called BK current is a Ca^{2+} and voltage-regulated potassium current has a steady and a transient components $I_{\mathrm{KBS,T}}$ with $V_{1/2} = -61.6$ mV. The noninactivating delayed-rectifier potassium current, I_{DRK}, has $V_{1/2} = -48.3$ mV. Four inward currents are: a voltage-gated Ca^{2+} current, I_{Ca}, with $V_{1/2} = -55$ mV; cation h-type current, I_{h}, with $V_{1/2} = -87$ mV; leak current, I_{L}; and MET current, I_{MET}. The membrane potential is given by

$$\begin{aligned}C_{\mathrm{m}}\frac{dV}{dt} &= -I_{\mathrm{K1}} - I_{\mathrm{BKS}} - I_{\mathrm{BKT}} - I_{\mathrm{DRK}} - I_{\mathrm{h}} \\ &\quad - I_{\mathrm{Ca}} - I_{\mathrm{L}} - I_{\mathrm{MET}},\end{aligned} \tag{3}$$

accompanied by equations for the gating variable and intracellular $[Ca^{2+}]$ totaling 12 coupled differential equations. A detailed description of these equations and parameters is provided in Ref. [44] and given in the Appendix. The maximum conductances for BK and K1 currents were used as control parameters.

In Eq. (3) the inward mechanoelectrical transduction current, I_{MET},

$$I_{\mathrm{MET}} = g_{\mathrm{MET}}P_{\mathrm{o}}(X, X_{\mathrm{a}})V, \tag{4}$$

serves as the forward coupling between mechanical and electrical compartments, and the MET conductance, g_{MET}, is the forward coupling strength. Positive deflection of the hair bundle leading to the MET channel opening results in depolarization of the cell.

To introduce the backward coupling, we sought to find a relation between the membrane potential and calcium concentration near myosin motor sites. The stall force, F_a, of the motors is calcium dependent and is approximated by a linear relation, $F_a = F_{\max}[1 - SP_{\mathrm{o}}(X, X_{\mathrm{a}})]$, where the calcium feedback strength S is defined as [13,24]

$$S = -\frac{[Ca^{2+}]_M}{F_{\max}}\frac{dF_a}{d[Ca^{2+}]}. \tag{5}$$

$[Ca^{2+}]_M$ is the Ca^{2+} concentration near the motor sites, which varies upon changing the membrane potential: more negative V results in a larger driving force on Ca^{2+}, leading to larger values of $[Ca^{2+}]_M$ and consequently to larger values of calcium feedback strength, S. The dependence of $[Ca^{2+}]_M$ versus V is calculated using the current Goldman-Hodgkin-Katz equation,

$$[Ca^{2+}]_M = \gamma[Ca^{2+}]_{\mathrm{ext}}\frac{\beta V}{1 - e^{\beta V}}, \quad \beta = \frac{2q_e}{k_BT}, \tag{6}$$

where $[Ca^{2+}]_{\mathrm{ext}}$ is extracellular Ca^{2+} concentration, γ is a dimensionless constant, and q_e is elementary charge. If S_0 is the calcium feedback strength at a reference potential, V_0, and $[Ca^{2+}]_{M0}$ is the Ca^{2+} concentration at motor sites at V_0, then S for any V can be written as

$$S = \frac{[Ca^{2+}]_M}{[Ca^{2+}]_{M0}}S_0. \tag{7}$$

Then using (6) we obtain

$$S(V) = S_0 \frac{V}{V_0} \frac{1 - e^{\beta V_0}}{1 - e^{\beta V}}. \quad (8)$$

In the following the reference membrane potential V_0 was set at $V_0 = -55$ mV as in Refs. [9,13]. For voltage variations in the range -80 to -30 mV, $S(V)$ in Eq. (7) can be linearized around V_0,

$$S(V) = S_0 \left[1 + \left(1 - \frac{\beta V_0}{1 - e^{-\beta V_0}} \right) \frac{V - V_0}{V_0} \right], \quad (9)$$

where the prefactor $1 - \frac{\beta V_0}{1 - e^{-\beta V_0}} = 0.9386$. In order to scale the effect of the membrane potential we introduce a dimensionless parameter α which accounts for the backward coupling strength in our model,

$$S(V) = S_0 \left[1 + \alpha \frac{V - V_0}{V_0} \right]. \quad (10)$$

Hyperpolarization of the cell below the reference potential, V_0, leads to an increase of the calcium feedback strength, S. This corresponds to increase of $[Ca^{2+}]_M$, resulting in closure of MET channels. Depolarization of the cell above V_0 results in decrease of S.

Equations (4) and (10) provide bidirectional coupling between the hair bundle dynamics (1) and the membrane potential (3). To conclude, the hair cell system is described by 14 differential equations. Its two compartments are coupled bidirectionally via Eqs. (4) and (10). Noise terms are included in the mechanical compartment only (1), as experimental studies showed that the MET current (4) is responsible for most of the fluctuations in saccular hair cells [41].

Bifurcation analysis of the *deterministic model* was carried out using the continuation software package CONTENT [55]. Numerical simulations were carried out using the Runge-Kutta method. To characterize synchronous dynamics of the deterministic compartments we have calculated a relative phase of compartments as follows. We extracted sequences of times of local minima for the hair bundle position, $t_x(j)$, and for the membrane potential, $t_v(k)$. The relative phase is then calculated by colocating the time of the hair bundle local jth minimum within the time interval of two consecutive minima of the membrane potential. Hence the relative phase is given by

$$\varphi(j) = \frac{t_x(j) - t_v(k)}{t_v(k+1) - t_v(k)}, \quad t_v(k) < t_x(j) < t_v(k+1). \quad (11)$$

A circle map is then constructed, $\varphi(j+1) = \Phi[\varphi(j)]$ [see Figs. 3(c) and 3(d)]. A sequence of fixed points in the circle map refers to a synchronous regime. A quasiperiodic regime corresponds to invariant curves in the map and can be distinguished from chaos by calculating the largest Lyapunov exponent (LE), which is 0 for quasiperiodic regimes and has positive values for chaos. The largest LE was calculated as in Ref. [44].

In the presence of noise the model equations were integrated using an Euler-Maruyama scheme with a fixed time step of 10^{-4} s [56]. Spontaneous stochastic dynamics was characterized by the power spectral densities (PSDs) of the hair bundle displacement and of the membrane potential, calculated from long (600 s) time series using the Welch periodogram method with Hamming window [57]. The quality factor, Q, of stochastic oscillations was estimated from the corresponding PSD as $Q = f_p/\Delta f_p$, where f_p is the peak frequency and Δf_p is the width of this peak at half maximal power.

Input-output relations of the stochastic model ($\epsilon = 1$) in response to the external stimulus force, F_{ext}, were characterized by two frequency-dependent sensitivity functions: "mechanical," χ_M, and "electrical," χ_V. For a sinusoidal external force,

$$F_{\text{ext}}(t) = F_0 \cos(2\pi f_s t), \quad (12)$$

these sensitivity functions are defined as in Refs. [6,13,44,60],

$$\chi_M(f_s) = |\tilde{X}(f_s)|/F_0, \quad \chi_V(f_s) = |\tilde{V}(f_s)|/F_0, \quad (13)$$

where f_s and F_0 are the stimulus frequency and amplitude, respectively; $|\tilde{X}(f_s)|$ and $|\tilde{V}(f_s)|$ are the magnitudes of the first Fourier harmonic of the time-dependent ensemble averages of the hair bundle position, $\langle X(t) \rangle$, and of the membrane potential, $\langle V(t) \rangle$. These time-dependent means were calculated by averaging an ensemble of 10^3 realizations of $X(t)$ and $V(t)$ over 500 periods of external sinusoidal force. In the linear response regime, i.e., for weak stimulus, $F_0 \leqslant 1$ pN, we used broad-band noise stimulation as in Ref. [44]. In this method $F_{\text{ext}} = s(t)$, where $s(t)$ is band-limited Gaussian noise with the variance σ_s^2 and cutoff frequency, f_c. The PSD of the stimulus is $G_{ss}(f) = \sigma_s^2/(2f_c)$ for frequencies within $[0\,, f_c]$ and 0 otherwise. In the following we used $f_c = 200$ Hz. The sensitivity functions are then defined as [57]

$$\chi_M(f) = \frac{|G_{sX}(f)|}{G_{ss}(f)}, \quad \chi_V(f) = \frac{|G_{sV}(f)|}{G_{ss}(f)}, \quad (14)$$

where $G_{sX}(f)$ is the cross-spectral densities between the stimulus and the hair bundle position, and $G_{sV}(f)$ is the cross-spectral density between the stimulus and the membrane potential. An obvious advantage of this method is that it allows estimation of sensitivity functions at all frequencies within the stimulus band at once for a given parameter setting, avoiding variation of the frequency of a sinusoidal force [44]. Figure 8 shows that both methods of sensitivity estimation coincide.

III. RESULTS

We study the role of voltage oscillations and coupling in spontaneous and response dynamics of the hair cell. We minimized the number of control parameters in the model by choosing those which result in pronounced change in the dynamics and can be controlled in an experiment. For mechanical compartment, we considered two fixed sets of parameters: (1) $S_0 = 1.13$, $F_{\max} = 55$ pN, at which the hair bundle is at stable equilibrium, but close to the Andronov-Hopf bifurcation [13], and (2) $S_0 = 0.66$, $F_{\max} = 50.2$ pN, at which the hair bundle is at a stable limit cycle, oscillating at a frequency of 8.5 Hz. Those regimes are observed for uncoupled hair bundle, when the EMT coupling strength $\alpha = 0$. Experimental studies have documented diverse voltage oscillatory patterns in bullfrog saccular hair cells which were correlated to distinct proportions of basolateral ion currents [40]. For example, large-amplitude oscillating cells are characterized by a larger fraction of K1 and a smaller fraction of BK

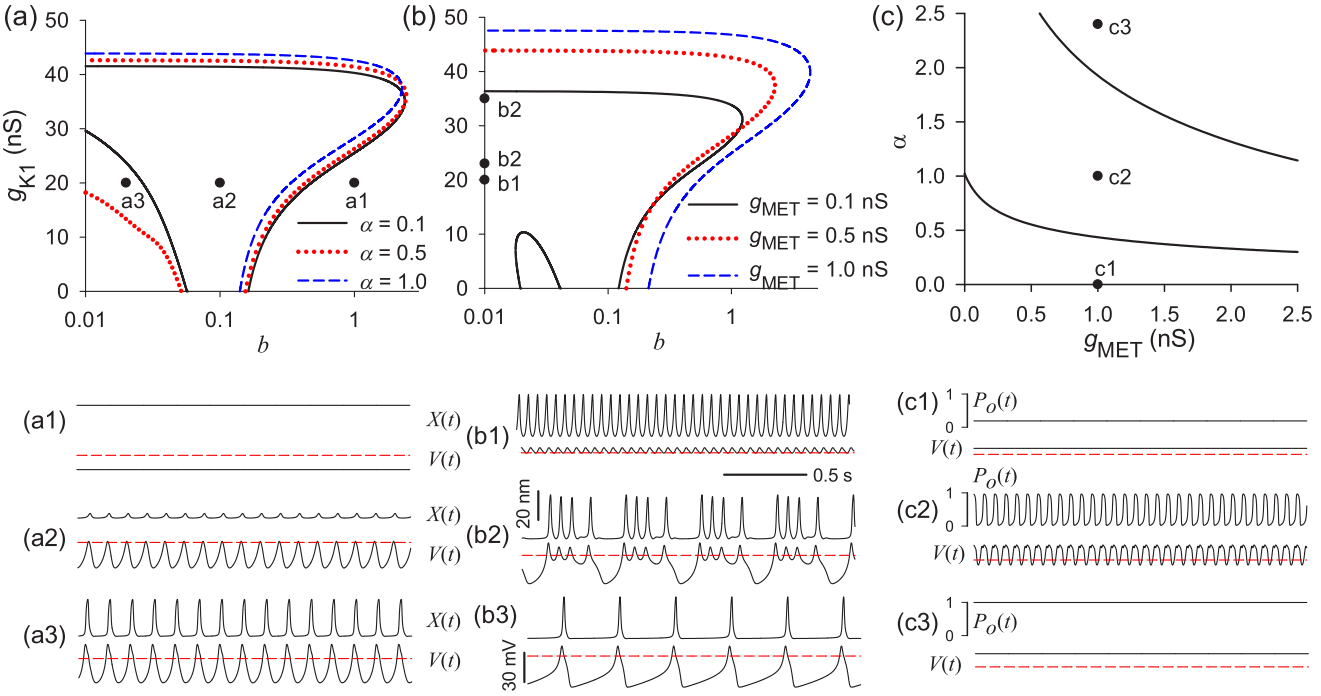

FIG. 2. (Color online) Dynamical regimes of the deterministic model for the case when the mechanical compartment is in a stable equilibrium state when uncoupled; $S_0 = 1.13$, $F_{max} = 55$ pN. (a), (b) Lines of Andronov-Hopf bifurcation on the parameter plane (b, g_{K1}) for indicated values of the coupling strengths (g_{MET} and α). In panel (a), $g_{MET} = 0.5$ nS; in panel (b), $\alpha = 1.0$. (c) Andronov-Hopf bifurcation lines on the parameter plane (g_{MET},α) for $b = 0.01$, $g_{K1} = 1$ nS, and other parameters being the same as in panels (a) and (b). Filled labeled circles correspond to the panels (a1)–(a3), (b1)–(b3), and (c1)–(c3). Each panel (a1)–(a3) and (b1)–(b3) shows time traces of the hair bundle position $X(t)$ (upper trace) and the membrane potential $V(t)$ (lower trace) for the parameters corresponding to the filled circles in panels (a) and (b). Upper traces in panels (c1)–(c3) show the open probability of MET channels, P_o. Dashed red line on lower traces in panels (a1)–(a3), (b1)–(b3), and (c1)–(c3) shows the reference voltage $V_0 = -55$ mV. Coupling strengths were fixed at $\alpha = 1$, $g_{MET} = 0.5$ nS for (a1)–(a3) and $\alpha = 1$, $g_{MET} = 0.1$ nS for (b1)–(b3).

currents. On the other hand, quiescent cells are correlated with a smaller fraction of K1 and a larger fraction of BK currents. Furthermore, oscillations in a quiescent cell can be induced by blocking BK currents [38,40]. Consequently, the parameters g_{K1} and b, which control the strengths of K1 and BK currents, were chosen as control parameters for the electrical compartment as in Ref. [44]. The experimentally reported range of the MET conductance, g_{MET}, is from 0.08 to 2.48 nS. Furthermore, MET channels can be blocked as in Ref. [40]. We therefore used g_{MET} as another control parameter for the strength of the forward mechanoelectrical coupling. Finally, a free parameter α was used to scale the backward electromechanical coupling.

The results are organized as follows. First, we describe deterministic dynamics of the hair cell system, concentrating on the effect of basolateral currents and coupling strengths on the onset of oscillations and their synchrony. Second, we study stochastic dynamics of the model when the hair bundle is subjected to fluctuations. Finally, we describe the response of the hair cell to weak mechanical forcing.

A. Deterministic dynamics

In the deterministic case $\epsilon = 0$ and $F_{ext} = 0$ in the mechanical compartment [Eqs. (1)]. We start with the case of a nonoscillating hair bundle. Lines of Andronov-Hopf (AH) bifurcation shown in Figs. 2(a) and 2(b) isolate the oscillation region on the parameter plane (b, g_{K1}) of the hair cell system. Within this region both the hair bundle and the membrane potential show oscillations [panels (a2), (a3), (b1)–(b3), and (c2) in Fig. 2]. Although the shape of the oscillation region is similar to that of the uncoupled electrical compartment [44], its size changes significantly with variation of the coupling strengths, α and g_{MET}.

An increase of the backward coupling, α, results in expansion of oscillation region towards smaller values of BK and K1 current strength [Fig. 2(a)]. For example, for $\alpha = 0.1$ [solid black curve in Fig. 2(a)] and small values of b and g_{K1}, the cell is at equilibrium with the potential V larger than the reference potential for the hair bundle ($V_0 = -55$ mV). An increase in α [e.g., dotted red curve in Fig. 2(a)] causes a decrease in $[Ca^{2+}]$ near molecular motors in the hair bundle via a decrease in the feedback parameter S (10), leading to the opening of MET channels and onset of hair bundle oscillations. This in turn activates oscillations in the electrical compartment due to forward coupling. The amplitude of oscillations becomes large for strong hyperpolarization of the cell [panel (b3) in Fig. 2], observed for large enough values of g_{K1}.

An increase of the forward coupling, g_{MET}, leads to an increase of the inward MET current, which depolarizes the cell, and so larger values of conductances of outward K currents are required to stabilize the cell at an equilibrium. This explains the expansion of the oscillation region with the increase of the MET conductance, g_{MET}, as shown in Fig. 2(b).

An important observation from Fig. 2 is that mechanical oscillations of the hair bundle are strongly influenced by the basolateral ionic currents. For example, an initially quiescent hair bundle at point A1 on Fig. 2(a) can oscillate [panels (a2) and (a3)] if BK currents are blocked, which corresponds to a decrease of the parameter b. Diverse oscillation patterns shown in panels (b1)–(b3) of Fig. 2 are observed for small strength of BK currents (small b). For the uncoupled electrical compartment these transitions were studied in detail in Ref. [44]. For fixed values of coupling strengths [Fig. 2(b)], the increase of the K1 current strength causes the membrane potential to depart from a low-amplitude oscillation [panel (b1)] to larger amplitude bursting oscillations, which have large and slow hyperpolarization excursions due to the h current, I_h [panel (b2)] [44]. Because of backward coupling the hair bundle also exhibits bursting patterns. We note, however, that this mechanical bursting differs from recently reported multimodal hair bundle oscillations [15] as in the latter work bursting was solely due to hair bundle dynamics, while in our case, it is the result of the backward electromechanical drive from the membrane potential. Further increase in g_{K1} results in a sequence of spike-adding bifurcations [44], in which the number of spikes per burst progressively decreases, ultimately leading to slow spiking oscillations [panel (b3)] and finally to a hyperpolarized rest potential at which the MET channels are in almost closed state.

The effect of coupling strength on the cell's dynamics is further illustrated in Fig. 2(c) where both compartments were at stable equilibrium in the absence of coupling ($\alpha = g_{MET} = 0$). The oscillating region on the parameter plane (g_{MET}, α) is bounded by AH bifurcation lines. For chosen parameters, below the lower bifurcation line in Fig. 2(c), the MET channels are in an almost closed state and the rest membrane potential is above the reference potential of the hair bundle, $V > V_0$ [panel (c1), Fig. 2]. For a fixed value of g_{MET} an increase in the backward coupling α results in oscillations of mechanical and consequently electrical compartments [panel (c2), Fig. 2], as explained above. Crossing the upper bifurcation line in Fig. 2(c) corresponds to the transition when MET channels are permanently in the open state, leading to a large MET current which puts the cell potential in a depolarized rest state [panel (c3)].

Next, we consider the effects of coupling on mechanical and electrical dynamics when both compartments are oscillating when uncoupled. The parameters of the hair bundle compartment were set at $S_0 = 0.66$ and $F_{max} = 50.18$ pN, resulting in stable limit cycle oscillations at 8.5 Hz, while the conductances of K1 and BK currents were varied within the oscillation region of the uncoupled ($g_{MET} = 0$) electrical compartment.

Bidirectional coupling leads to synchronization of self-sustained oscillators [58], which was quantified using circle maps built from time sequences of local extrema in the hair bundle position $X(t)$ and the membrane potential $V(t)$. Stable fixed points in such maps indicate phase-locked synchronous dynamics of the model compartments. Quasiperiodic dynamics is reflected by continuous lines in the map [see, e.g. Fig. 3(c)]. The coupling strength resulting in phase and frequency locking depends on frequency detuning of interacting oscillators. Figure 3 shows the results of coupling strengths sweeping for representative examples of weakly and strongly detuned mechanical and electrical compartments. Weakly detuned compartments [Fig. 3(a)] are phase locked for rather small values of MET conductance, so that for $g_{MET} > 0.1$ nS the hair bundle motion and the voltage variations are phase and frequency locked across large regions of the backward coupling strength, α. Smaller coupling results in multiple synchronization regions separated by regions quasiperiodic motion [white areas in Fig. 3(a)] and small regions of chaos [black areas in Fig. 3(a)]. Figure 3(b) exemplifies the case of large detuning when the uncoupled electrical compartment is in the regime of large-amplitude low-frequency spiking oscillations resulting by raising K1 current conductance and lowering the BK current conductance. For small values of BK current strength, b, the uncoupled electrical compartment demonstrates structurally unstable dynamics for increasing values of g_{K1} with sequences of spike-adding bifurcations in bursting oscillations [44]. Effective backward coupling is strong in this case, resulting in extensive chaotic regions and absence of quasiperiodicity [Fig. 3(b)], which is consistent with the dynamics of a supercritical circle map [58]. Similar to the case of weak detuning, starting with $g_{MET} = 0.3$ nS compartments are phase locked across for the entire range of backward coupling strength, α. The oscillation region on the coupling strengths' parameter plane (g_{MET}, α) is bounded by the AH bifurcation line, which indicates oscillation quenching [58], so that beyond this line both compartments are at rest with MET channels in an open state and a depolarized rest membrane potential.

B. Stochastic spontaneous dynamics

In the hair cell model noise enters into the hair bundle compartment when the parameter $\epsilon = 1$. Noise could induce hair bundle oscillations even when the cell is in nonoscillating deterministic regimes. This is demonstrated in Fig. 4, which should be compared with its deterministic counterpart in Fig. 2(c). In the absence of backward electromechanical coupling ($\alpha = 0$) the cell is at stable equilibrium. Noise induces sporadic oscillations of the hair bundle followed by voltage variations due to MET current [panel (a1), Fig. 4]. These noise-induced oscillations are characterized by a broad peaks in the PSDs of mechanical and electrical compartments [dashed red lines in Fig. 4(b) and 4(c)], notably centered at distinct frequencies. An increase of α moves the system into the oscillation region [see Fig. 2(c)]. As a result, oscillations of both compartments become more coherent as seen in time traces of panel (a2) in Fig. 4. Corresponding PSDs show sharp narrow peaks at the same frequencies in both compartments [solid green lines in Figs. 4(b) and 4(c)]. Further increase of backward coupling strength α beyond the oscillation region ceases oscillations [panel (a3) in Fig. 4]. The quality of oscillations in both compartments is maximal in the middle of the oscillation region bounded by AH bifurcation lines in Fig. 2(c).

The coherence of stochastic oscillations depends crucially on the parameters of the electrical compartment, as variation of basolateral ionic currents strength can promote self-sustained oscillations of an initially quiescent cell [see Fig. 2(a)]. Figure 5 demonstrates that blocking of BK currents may result in dramatic increase of oscillation coherence. For large BK

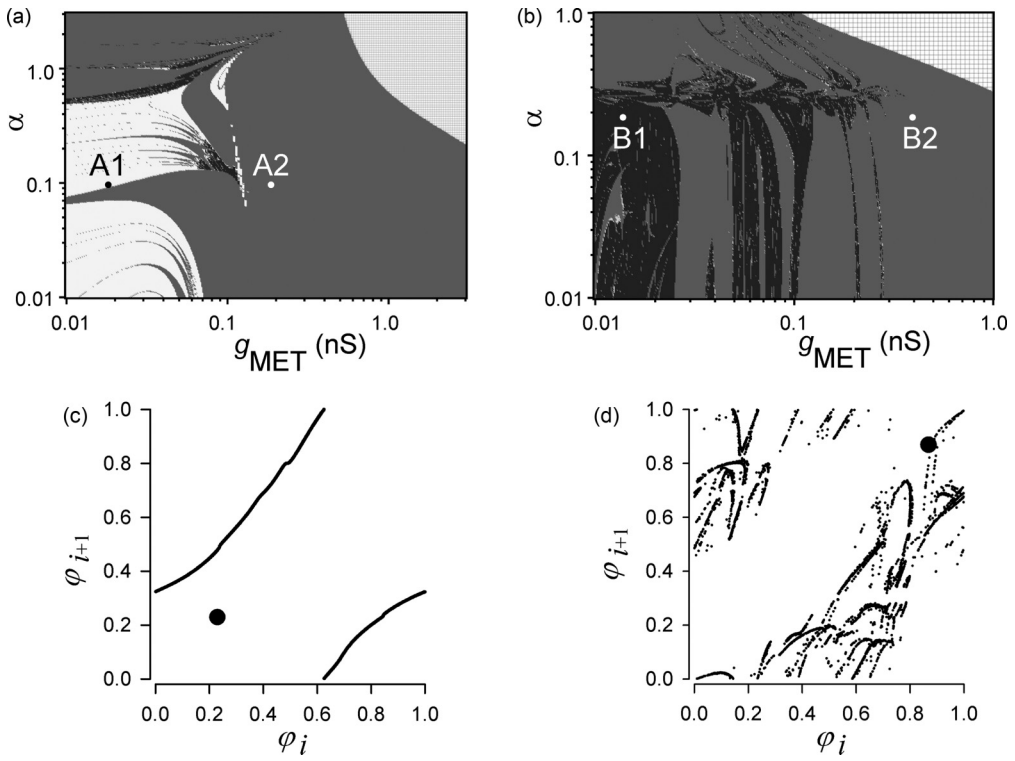

FIG. 3. Synchronization of the hair cell model compartments. (a), (b) Regions of synchronization (dark gray), quasiperiodic motion (white), chaotic (black), and quiescent (patterned) on the coupling strengths' parameter plane (g_{MET}, α). The parameters of the hair bundle compartment are fixed at $S_0 = 0.66$, $F_{max} = 50.18$ pN in both panels. In panel (a) the parameters of electrical compartment, $g_{K1} = 10$ nS and $b = 0.1$, resulted in 9 Hz small-amplitude voltage oscillations in the absence of coupling, $g_{MET} = 0$. In panel (b), $g_{K1} = 25$ nS and $b = 0.01$ resulted in large-amplitude spiking oscillations at a lower frequency of 4.5 Hz. Filled black labeled circles in panels (a) and (b) correspond to circle maps shown in panels (c) and (d). (c), (d) Circle maps, $\varphi_{i+1} = \Phi(\varphi_i)$, for the marked points in panels (a) and (b). Filled large circles indicate 1:1 phase locked regimes, corresponding to points A2 and B2 in panels (a) and (b). Lines in the circle map in panel (c) and complicated structures in panel (d) refer to quasiperiodic and chaotic oscillations, corresponding to points A1 and B1 in panels (a) and (b), respectively.

current strength ($b = 1$) the cell was in a quiescent state [traces (a1) in Fig. 2]. Noise induces noncoherent oscillations in both compartments [panel (a1) in Fig. 5], which are characterized by wide peaks in corresponding PSDs [dashed black lines in Figs. 5(b) and 5(c)]. A decrease in b, corresponding to blocking of BK currents, leads to large-amplitude coherent oscillations [panel (a2) in Fig. 5] reflected by large and narrow peaks in the PSDs [solid red lines in Figs. 5(b) and 5(c)].

We now turn to the case when both cells' compartments are oscillating at similar natural frequencies when uncoupled, referring to the deterministic case shown in Fig. 3(a). With noise added, the mechanical compartment represents a low-quality oscillator, coupled to a noiseless electrical compartment, potentially a high-quality oscillator. According to the theory of coupled self-sustained stochastic oscillators, bidirectional coupling of such distinct oscillators may improve

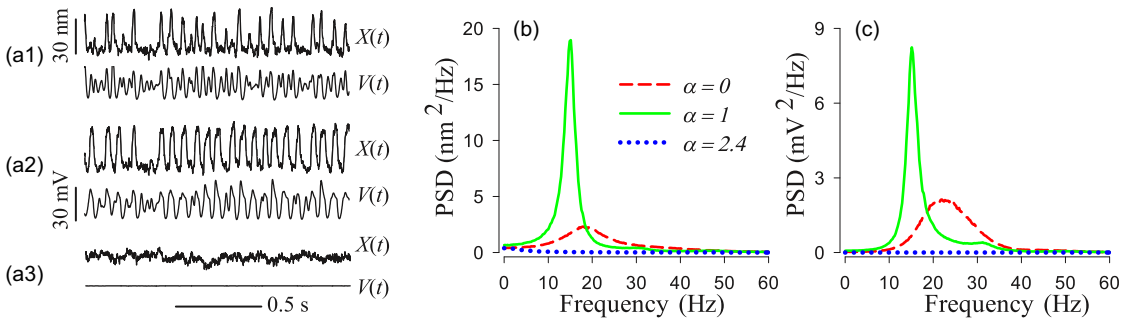

FIG. 4. (Color online) Stochastic spontaneous dynamics of an initially quiescent hair cell system for different values of the backward coupling strength, α. The parameters of the hair bundle compartment are $S_0 = 1.13$, $F_{max} = 55$ pN; and $b = 0.01$, $g_{K1} = 1$ nS for the electrical compartment; the forward coupling strength, $g_{MET} = 1$ nS. (a1)–(a3): Time traces for the hair bundle position, $X(t)$, and the membrane potential, $V(t)$; $\alpha = 0$ in (a1), $\alpha = 1$ in (a2), and $\alpha = 2.4$ in (a3). These parameter values are the same as in Fig. 2(c). (b), (c) Power spectral densities (PSDs) of the hair bundle position (b) and of the membrane potential (c).

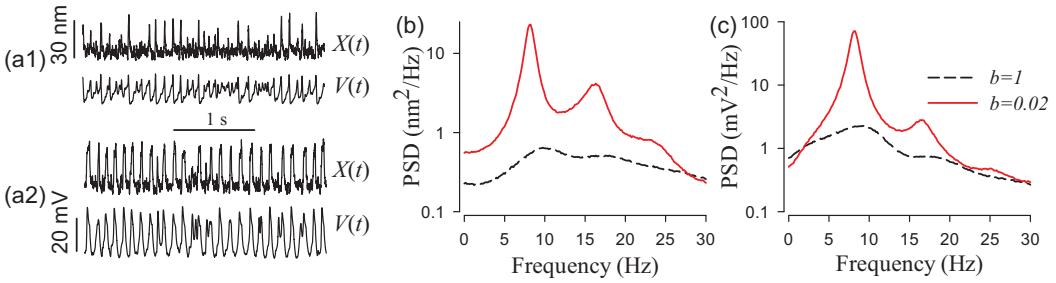

FIG. 5. (Color online) Stochastic spontaneous dynamics of the hair cell system for two values of BK current strength. The parameters of the mechanical compartment are $S_0 = 1.13$, $F_{max} = 55$ pN, and $g_{K1} = 1$ nS, for the electrical compartment; the coupling strengths are $g_{MET} = 0.5$ nS, $\alpha = 0.5$. (a1)–(a2): Time traces for the hair bundle position, $X(t)$, and the membrane potential, $V(t)$; $b = 1$ for (a1), $b = 0.02$ for (a2). (b), (c) PSDs of the hair bundle position (b) and of the membrane potential (c).

their coherence if the coupling strength from low-noise to high-noise oscillators is larger than that from a high-noise to low-noise oscillator [58,59]. Backward electromechanical coupling from a high-quality somatic oscillator to a low-quality noisy hair bundle oscillator may then improve overall quality of oscillations. On the other hand, forward mechano-electrical coupling brings stochasticity from the mechanical compartment to the electrical compartment, which could presumably worsen oscillations quality. The example shown in Fig. 6 demonstrates this effect. For a fixed small forward coupling strength, g_{MET}, the increase of backward coupling strength, α, leads to narrower peaks in the PSDs [Figs. 6(a) and 6(b)]. This increase in the coherence of the the oscillations is quantified by the quality factor as shown in Figs. 6(c) and 6(d). The effect becomes less pronounced for larger values of g_{MET} and disappears for $g_{MET} = 0.5$ nS. As predicted by the theory, oscillation coherence decreases with increase of forward coupling, g_{MET}: quality factors of mechanical and electrical oscillations decrease when g_{MET} increases, as shown in Fig. 6(e). We note that while the backward coupling strength is a rather artificial parameter, the strength of MET current, i.e., the strength of forward coupling, can be altered in an experiment by blocking the inward MET current as in Ref. [34].

Finally we consider two highly detuned oscillating compartments as shown in Fig. 3(b). For weak forward coupling, compartments show distinct stochastic dynamics: the hair bundle oscillates at 10 Hz, while the membrane potential shows large-amplitude, low-frequency intermittency between spikes and bursts at 4.5 Hz [Fig. 7(a1)]. Figure 7(b) shows two

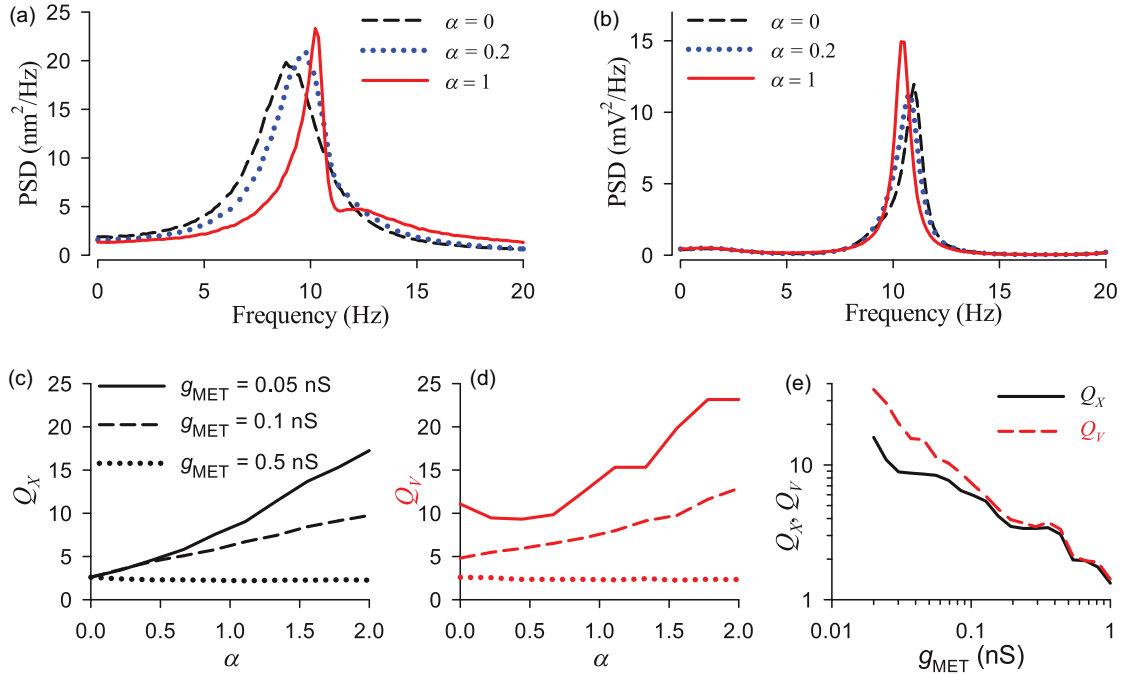

FIG. 6. (Color online) Effect of coupling on a spontaneously oscillating hair cell with closely tuned compartments. The parameters of the mechanical compartment are $S_0 = 0.66$, $F_{max} = 50.18$ pN, and $b = 0.1$, $g_{K1} = 10$ nS, for the electrical compartment. (a), (b) PSDs of the hair bundle position (a) and of the membrane potential (b) for $g_{MET} = 0.05$ and indicated values of backward coupling strength, α. (c), (d) Quality factor of the hair bundle oscillations [Q_X, panel (c)] and of the membrane potential [Q_V, panel (d)] versus α for the indicated values of forward mechanoelectrical coupling strength, g_{MET} (dotted, dashed, and solid lines). (e) Quality factors of mechanical (solid black curve) and electrical (dashed red curve) oscillations versus g_{MET} for the fixed $\alpha = 1$.

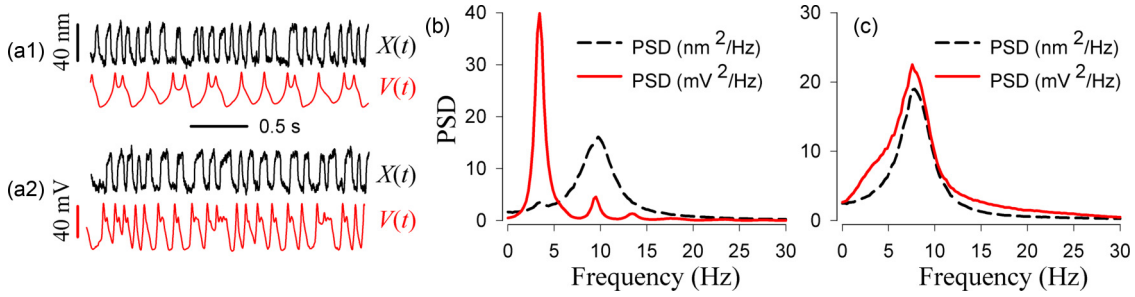

FIG. 7. (Color online) Frequency locking of detuned hair cell compartments. The parameters are $S_0 = 0.66$, $F_{\max} = 50.18$ pN, and $b = 0.01$, $g_{K1} = 25$ nS; backward coupling strength, $\alpha = 0.2$. (a1)–(a2): Time traces for the hair bundle position, $X(t)$ (black lines), and the membrane potential, $V(t)$ for small [$g_{MET} = 0.015$ nS, (a1)] and strong [$g_{MET} = 0.3$ nS, (a2)] coupling. (b), (c) PSDs of the hair bundle position (dashed black lines) and of the membrane potential (solid red lines) corresponding to time traces in panel (a1) and (a2).

distinct peaks in their corresponding PSDs. With increased forward coupling, oscillations in both compartments become synchronous [Fig. 7(b)] with frequencies locked at 7.5 Hz, as indicated by PSDs of both compartments, shown in Fig. 7(c), peaked at this frequency.

C. Response dynamics

Input-output relations of the hair cell system were probed with two types of external mechanical forces: sinusoidal, $F_{ext}(t) = F_0 \sin(2\pi f_s t)$, and broad-band Gaussian noise, as explained in Methods. The sensitivity functions estimated for weak mechanical stimuli were peaked at the natural frequencies of the cell's compartments. Figure 8 shows a representative example of sensitivity functions for the case when both deterministic compartments were not oscillating when uncoupled (cf. Fig. 4 for spontaneous dynamics). With no backward coupling, $\alpha = 0$, the sensitivity functions are broad, centered at distinct frequencies [Figs. 8(a) and 8(b)]. Transition to the oscillating region for $\alpha = 1$ is characterized by higher and sharper sensitivity functions, peaking at the same frequency. Further increase of backward coupling strength moves the system closer to the upper bound of the oscillation region [Fig. 2(c)] and thus decreases the sensitivity of both compartments. Similar behavior of the sensitivity is observed for varying forward coupling, g_{MET}, and fixed α. Sensitivity over the whole frequency domain is maximal for intermediate values of coupling strengths in the middle of oscillation region in Fig. 2(c). Approaching the AH bifurcation lines turns the system more susceptible to internal noise, which worsens its sensitivity to the external mechanical force.

For large-amplitude stimuli the response of the hair cell becomes nonlinear. In particular the hair bundle demonstrates the phenomenon of compressive nonlinearity [6,13,60], whereby sensitivity is enhanced for weak stimuli and suppressed for strong stimuli. Figure 8(c) demonstrates that the compressive nonlinearity is preserved for the hair cell system with coupled mechanical and electrical compartments. In particular, the hair bundle sensitivity shows qualitatively the same dependence versus the stimulus amplitude as reported before for the hair cell model with *fixed* membrane potential [13]: the response is linear for weak, $F_0 < 1$ pN, and very large, $F_0 > 100$ pN, stimulus amplitude and is nonlinear for intermediate values. The sensitivity of the electrical compartment does not saturate for large F_0, and the response continues to be nonlinear.

Variations of basolateral ionic currents strength affect significantly the response dynamics of the hair cell. Figure 9 shows the sensitivity functions of a cell which was initially nonoscillating (cf. Fig. 5). For relatively strong BK currents ($b = 1$) when spontaneous activity of the cell is solely due to noise-induced oscillations of the hair bundle, the sensitivities

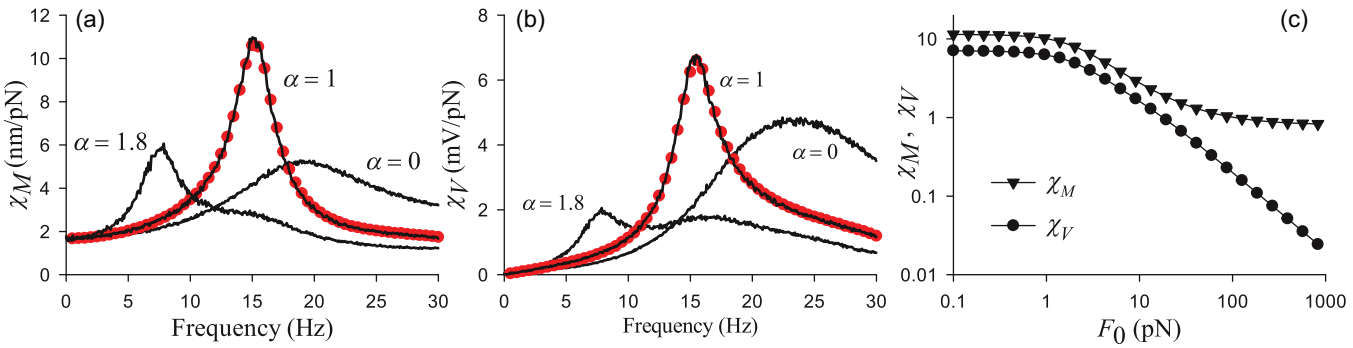

FIG. 8. (Color online) Sensitivity of the hair cell system for different values of the backward coupling strength, α. The parameters of the hair cell compartments are $S_0 = 1.13$, $F_{\max} = 55$ pN; $b = 0.01$, $g_{K1} = 1$ nS. The forward coupling strength is $g_{MET} = 1$ nS. (a), (b) Sensitivity of the hair bundle (χ_M, a) and of the membrane potential (χ_V, b) to noise stimulus with the standard deviation, $F_0 = 1$ pN for the indicated values of the backward coupling strength α. For comparison, filled red (dark gray) circles show the sensitivities calculated for sinusoidal external force with the amplitude $F_0 = 0.5$ pN. (c) Sensitivity functions for the hair bundle and the membrane potential versus the amplitude of sinusoidal stimulus at stimulus frequency, $f_s = 15$ Hz for $\alpha = 1$.

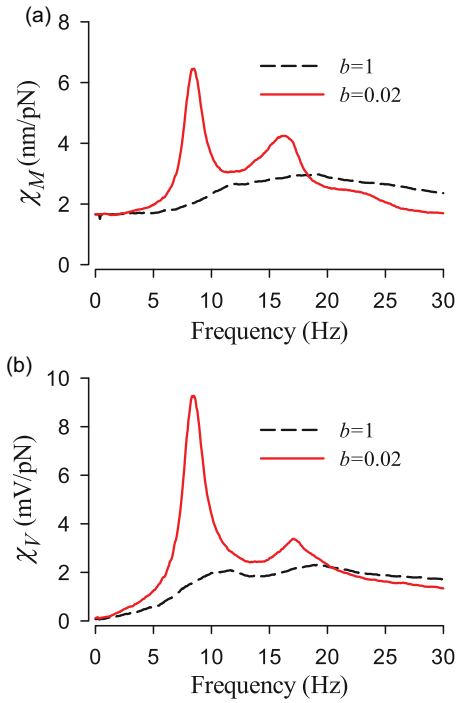

FIG. 9. (Color online) Sensitivity functions of the hair cell system for the indicated values of BK current strengths. The parameters are the same as in Fig. 5, except that external broad-band Gaussian noise stimulus with the standard deviation $F_0 = 1$ pN is applied to the mechanical compartment. (a) Sensitivity function of the hair bundle, χ_M. (b) Sensitivity function of the somatic potential, χ_V.

of both compartments attain low values and are characterized by broad frequency distributions (solid black lines in Fig. 9). Suppressing of BK currents ($b = 0.02$) renders the cell in an oscillation region, boosting its sensitivity and frequency selectivity, as evidenced by sharp sensitivity functions of both compartments (dashed red lines in Fig. 9).

Cells with detuned oscillatory mechanical and electrical compartments show a general response trend, exemplified in Fig. 10. For a weak coupling, the sensitivity functions show two main peaks corresponding to natural frequencies of the hair bundle and the membrane potential [solid green lines in Figs. 10(a) and 10(b)]. The increase of forward coupling strength, g_{MET}, leads to frequency locking (cf. Fig. 7), resulting in larger and sharper sensitivity functions [dashed black lines in Figs. 10(a) and 10(b)]. Further increase of coupling strength moves the cell out of the oscillation region [see Fig. 3(b)], which results in suppression of the sensitivity function [dotted red lines in Figs. 10(a) and 10(b)]. For the somatic potential the maximal sensitivity across the whole frequency band thus becomes a nonmonotonous function of the MET conductance, taking its maximum at intermediate values of g_{MET}, as shown in Fig. 10(c). The effect is observed for large enough values of backward coupling strength, α, as well as for cells with closely tuned compartments. We note that the MET conductance can be altered in an experiment [34], so that this model prediction can be verified in an experiment.

We note that for a sensor composed of two unidirectionally coupled linear cascades it is expected that the response at the output of the second cascade would increase with the coupling strength between cascades, as more stimulus power entering the first cascade will become available for the second cascade [57]. This tendency is indeed observed in the hair cell model for small coupling strengths. However, besides a transformed stimulus, the MET current, which is proportional to g_{MET}, brings to the somatic electrical compartment stochastic variability from the noisy hair bundle as well. This variability is then fed back to the mechanical compartment by backward electromechanical transduction, which suppresses the sensitivity for strong enough coupling strengths [Fig. 10(c)].

IV. CONCLUSIONS

We studied spontaneous and response dynamics of a hair cell model which incorporates a nonlinear stochastic hair bundle oscillator and a Hodgkin-Huxley-type system of basolateral ionic currents. We focused in particular on the role of bidirectional mechanoelectrical and electromechanical coupling between these two compartments and on the role of voltage dynamics on the emergence of oscillations, their coherence, and amplification properties of the cell.

We have isolated oscillation regions bounded by the lines of Andronov-Hopf bifurcations in the parameter space of the model. Our results show that the hair bundle alters its dynamical state in response to membrane potential variations, and that changes in forward and backward coupling strengths

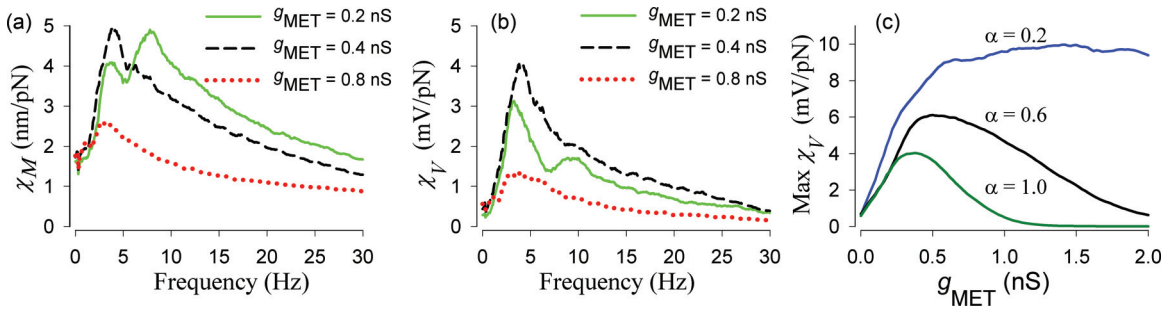

FIG. 10. (Color online) Effect of coupling strengths on sensitivity functions. The parameters of the cell's compartment, S_0, F_{max}, b, and g_{K1}, are the same as in Fig. 7. External broad-band Gaussian noise stimulus with the standard deviation $F_0 = 1$ pN is applied to the mechanical compartment. (a), (b) Sensitivity functions of the hair bundle, χ_M, and of the somatic potential, χ_V, for $\alpha = 1$ and indicated values of g_{MET}. (c) Maximal value of the sensitivity function of somatic potential across the whole frequency band versus g_{MET} for the indicated values of backward coupling strength, α.

may revert nonoscillating hair bundle to oscillatory ones, and vice versa. Furthermore, oscillatory hair cells exhibit spiking, bursting, and chaotic patterns in response to variations of coupling strengths and of conductances of basolateral ionic currents. Even for a relatively weak forward coupling ($g_{MET} > 0.1$ nS) oscillations of hair bundles and membrane potential are synchronized. For large coupling strengths oscillation quenching takes place, at which mechanoelectrical transduction channels are mostly in the open state while the cell is depolarized. Thus, a balance between these coupling strengths is needed in order to keep the cell in self-sustained oscillatory states.

The model has a limitation in that it does not demonstrate the specific bursting pattern observed for free-standing hair bundles [15,34]. These multimodal oscillations are characterized by large and extremely slow negative excursions of the hair bundle, which disappear when the hair bundle is loaded. Such multimodal dynamics require an additional slow variable in the hair bundle model, e.g., slow modulation of the gating spring stiffness proposed in Ref. [15]. The hair bundle model which is used here does not include this additional slow variable. Rather, it assumes a stimulation fiber attached to the hair bundle and thus an external mechanical load [13]. Consequently, a bursting pattern generated by the model [panel (b2), Fig. 2] is solely due to strong backward electromechanical coupling, whereby bursting of the membrane potential drives the hair bundle dynamics.

Spontaneous dynamics of the hair cell is inherently noisy mainly due to fluctuations of the hair bundle compartment [41]. In the model stochastic terms were incorporated in the hair bundle compartment which fed a fluctuating mechanoelectrical transduction current to the electrical compartment. The coherence of mechanical and electrical spontaneous oscillations depends crucially on the coupling strengths and on the conductances of the basolateral ionic currents. In particular the model predicts that for weak forward mechanoelectrical coupling (small values of g_{MET}) the coherence of spontaneous oscillations can be enhanced by backward electromechanical coupling (Fig. 6). Our results indicate that spontaneous noisy oscillations of hair bundles routinely reported in experimental studies can result from nonlinear interaction of mechanical and electrical compartments of the hair cell. This is supported by a recent experimental study where drastic changes of hair bundle oscillations in response to basolateral ion channel blockage were reported [34]. The model shows qualitative agreement with these experimental observations, exemplified in Fig. 11. Blocking of the calcium-activated potassium channels (BK) and the delayed rectifier potassium current (DRK) activates large-amplitude low-frequency voltage oscillations, causing high-frequency mechanical oscillations to slow down and increases their amplitude [Fig. 11(a)]. An initially quiescent hair bundle [Fig. 11(b)] starts oscillating when the cell becomes depolarized upon blockage of BK and DRK ion currents. Alongside these observations, our model shows that blocking of calcium-activated potassium channels alone induces large-amplitude coherent oscillations as shown in Fig. 5, enhancing the coherence of oscillations, and renders the cell more sensitive and frequency selective (see Fig. 9).

The main characteristics of the active hair bundle, such as compressive nonlinearity and frequency selectivity, are reproduced by the two-compartment model. Both compartments showed frequency selectivity, sensitivity, and compressive nonlinearity for incoming mechanical stimuli with amplitudes greater than 1 pN. However, while the mechanical hair bundle showed saturated response for stimuli greater than 100 pN, the electrical compartment sustained its compressive response for large (>100 pN) stimuli. An important issue of the exponent of nonlinear compression [60] was not studied here. In particular, an interesting question of how the exponent of nonlinear compression depends on the coupling strengths and detuning of the cell compartments will be addressed elsewhere. In this respect we refer to the theoretical study [46], where this question was addressed in a deterministic hair cell model for the case of weak coupling.

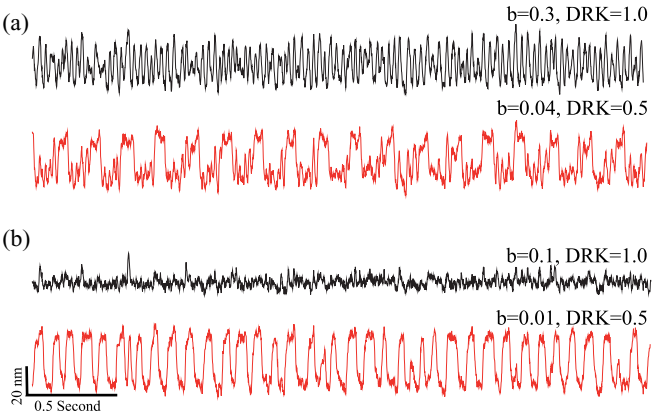

FIG. 11. (Color online) Effect of ion channels blockers on spontaneous oscillations of the hair bundle in the model. Black traces show the original dynamics of the hair bundle, while red traces show the dynamics after two types of ionic currents, the calcium-activated potassium current (I_{BK}) and the delayed rectifier current (I_{DRK}), were blocked. The strength of I_{BK} is controlled by the parameter b, and I_{DRK} is controlled by the parameter DRK in Eq. (A4). Higher values of these parameters correspond to larger currents. The parameter values are for panel (a) $S_0 = 0.9$, $F_{max} = 75$ pN, $g_{K1} = 7.5$ nS, $g_L = 0$, $\alpha = 1.6$, $g_{MET} = 0.1$ nS, and for panel (b) $S_0 = 1.4$, $F_{max} = 55$ pN, $g_{K1} = 7.5$ nS, $g_L = 0$, $\alpha = 1.6$, $g_{MET} = 0.1$ nS.

Noise is the limiting factor of the hair bundle sensitivity [13,60]. We find that the sensitivity to weak stimuli can be maximized by adjusting the interaction between hair cell compartments. For a cell whose uncoupled compartments are at equilibrium, the sensitivity can be maximized in the middle of oscillatory region bounded by the lines of Andronov-Hopf bifurcations [Figs. 2(c) and 8]. That is, variation of both the forward and backward coupling can maximize the sensitivity. However, for a cell with oscillating uncoupled compartments the maximal sensitivity depends nonmonotonously on the MET conductance in the presence of backward electromechanical coupling (see, e.g., Fig. 10), while the reverse electromechanical transduction degrades the sensitivity. This shows that stochastic hair bundle oscillations limit sensitivity of the hair cell.

ACKNOWLEDGMENTS

This work was supported by the Condensed Matter and Surface Science Program and the Quantitative Biology Institute

at Ohio University. The authors thank A. L. Shilinikov, D. F. Russell, and M. H. Rowe for valuable discussions.

APPENDIX: MEMBRANE POTENTIAL MODEL

The membrane potential is given by

$$C_m \frac{dV}{dt} = -I_{K1} - I_{BKS} - I_{BKT} - I_{DRK} - I_h - I_{Ca} - I_L - I_{MET}, \quad \text{(A1)}$$

where $C_m = 10$ pF is the membrane capacitance. Equations for each individual current are given below.

The inwardly rectifier current (I_{K1}) [38] is given by

$$\begin{aligned} I_{K1} &= g_{K1}[0.7\, m_{K1f}(V) + 0.3\, m_{K1s}(V)](V + 95), \\ \tau_{K1f,s} \frac{dm_{K1f,s}}{dt} &= k m_{K1\infty} - m_{K1f,s}, \\ m_{K1\infty} &= \{1 + \exp[(V + 110)/11]\}^{-1}, \\ \tau_{K1f} &= 0.7 \exp[-(V + 120)/43.8] + 0.04, \\ \tau_{K1s} &= 14.1 \exp[-(V + 120)/28] + 0.04, \end{aligned} \quad \text{(A2)}$$

where g_{K1} is the maximum conductance, and used as a control parameter.

The cation h current (I_h) [38] is given by

$$\begin{aligned} I_h &= g_h \left[3m_h^2(1 - m_h) + m_h^3\right](V + 45), \\ \tau_h \frac{dm_h}{dt} &= m_{h\infty} - m_h, \\ m_{h\infty} &= \{1 + \exp[(V + 87)/16.7]\}^{-1}, \\ \tau_h &= 63.7 + 135.7 \exp\left[-\left(\frac{V + 91.4}{21.2}\right)^2\right], \end{aligned} \quad \text{(A3)}$$

where $g_h = 2.2$ nS is the maximal conductance.

The delayed rectifier current (I_{DRK}) [61] is given by

$$\begin{aligned} I_{DRK} &= \text{DRK}\ P_{DRK} \frac{VF^2}{RT} \frac{0.112 - 0.002\, e^{-FV/RT}}{1 - e^{-FV/RT}} m_{DRK}^2, \\ \tau_{DRK} \frac{dm_{DRK}}{dt} &= m_{DRK\infty} - m_{DRK}, \\ m_{DRK\infty} &= \{1 + \exp[(V + 48.3)/4.19]\}^{-1/2}, \\ \tau_{DRK} &= (\alpha_{DRK} + \beta_{DRK})^{-1}, \\ \alpha_{DRK} &= (3.2\, e^{-V/20.9} + 3)^{-1} \\ \beta_{DRK} &= (1467\, e^{V/5.96} + 9)^{-1}, \end{aligned} \quad \text{(A4)}$$

where $P_{DRK} = 2.4 \times 10^{-14}$ L/s is the maximum permeability, and F and R are the Faraday and universal gas constants, respectively. The parameter DRK = 1 was kept fixed in this study, except for Fig. 11.

The voltage-gated Ca^{2+} current (I_{Ca}) [61] is given by

$$\begin{aligned} I_{Ca} &= g_{Ca} m_{Ca}^3 (V - 42.5), \\ \tau_{Ca} \frac{dm_{Ca}}{dt} &= m_{Ca\infty} - m_{Ca}, \\ m_{Ca\infty} &= \{1 + \exp[-(V + 55)/12.2]\}^{-1}, \\ \tau_{Ca} &= 0.046 + 0.325 \exp\left[-\left(\frac{V + 77}{51.67}\right)^2\right], \end{aligned} \quad \text{(A5)}$$

where $g_{Ca} = 1.2$ nS.

The Ca^{2+}-activated potassium current (BK) has a steady (BKS) and a transient (BKT) component [38]:

$$\begin{aligned} I_{BKS} &= b P_{BKS} \frac{VF^2}{RT} \frac{0.112 - 0.002\, e^{-FV/RT}}{1 - e^{-FV/RT}} (O_2 + O_3), \\ I_{BKT} &= b P_{BKT} \frac{VF^2}{RT} \frac{0.112 - 0.002\, e^{-FV/RT}}{1 - e^{-FV/RT}} (O_2 + O_3)\, h_{BKT}, \end{aligned} \quad \text{(A6)}$$

where $P_{BKS} = 2 \times 10^{-13}$ L/s, and $P_{BKT} = 14 \times 10^{-13}$ L/s are the BK currents' respective maximum permeabilities. Dimensionless parameter b was used to control the strength of the BK currents. I_{BKS} has an an additional inactivation gate, whose dynamics are described by [38]

$$\begin{aligned} \tau_{BKT} \frac{dh_{BKT}}{dt} &= h_{BKT\infty} - h_{BKT}, \\ h_{BKT\infty} &= [1 + \exp((V + 61.6)/3.65)]^{-1}, \\ \tau_{BKT} &= 2.1 + 9.4 \exp\{-[(V + 66.9)/17.7]^2\}. \end{aligned} \quad \text{(A7)}$$

The kinetic scheme of BK currents and $[Ca^{2+}]$ dynamics [62] is given by

$$\begin{aligned} \frac{dC_1}{dt} &= k_1[Ca^{2+}]C_0 + k_{-2}C_1 - (k_{-1} + k_2[Ca^{2+}])C_1, \\ \frac{dC_2}{dt} &= k_2[Ca^{2+}]C_1 + \alpha_c O_2 - (k_{-2} + \beta_c)C_2, \\ \frac{dO_2}{dt} &= \beta_c C_2 + k_{-3} O_3 - (\alpha_c + k_3[Ca^{2+}])O_2, \\ \frac{dO_3}{dt} &= k_3[Ca^{2+}]O_2 - k_{-3} O_3, \\ \frac{d[Ca^{2+}]}{dt} &= -0.00061 I_{Ca} - 2800[Ca^{2+}], \end{aligned} \quad \text{(A8)}$$

where $C_0 = 1 - (C_1 + C_2 + O_2 + O_3)$, $k_j = k_{-j} / [k_j(0) e^{-\delta_j \frac{FV}{RT}}]$, $j = 1,2,3$, and $\alpha_c = \alpha_c(0) e^{\frac{V}{V_A}}$. The channel opening rate constant was set to $\beta_c = 2500\ s^{-1}$. The rest of the parameters in Eq. (A8) are the same as in Ref. [62]: $k_1(0) = 6$ μM, $k_2(0) = 45$ μM, $k_3(0) = 20$ μM; $k_{-1} = 300$ s^{-1}, $k_{-2} = 5000$ s^{-1}, $k_{-3} = 1500$ s^{-1}; $\alpha_c(0) = 450$ s^{-1}, and $V_A = 33$ mV. The constants $\delta_1 = \delta_3 = 0.2$, and $\delta_2 = 0$.

The leak current (I_L) is given by

$$I_L = g_L V, \quad \text{(A9)}$$

where $g_L = 0.1$ nS.

The mechanoelectrical transduction current (I_{MET}) is given by

$$I_{MET} = g_{MET} P_o(X, X_a) V, \quad \text{(A10)}$$

where the maximum conductance of MET channels g_{MET} serve as the forward coupling strength and the open probability of MET channels, $P_o(X, X_a)$, is given by Eq. (2). In Eqs. (A9) and (A10) the reversal potential of MET and leak currents were set to 0 mV as in Ref. [42].

[1] J. Ashmore, P. Avan, W. Brownell, P. Dallos, K. Dierkes, R. Fettiplace, K. Grosh, C. Hackney, A. Hudspeth, F. Jülicher, B. Lindner, P. Martin, J. Meaud, C. Petit, J. Sacchi, and B. Canlon, Hearing Res. **266**, 1 (2010).

[2] A. Hudspeth, Neuron **59**, 530 (2008).

[3] A. J. Hudspeth, F. Jülicher, and P. Martin, J. Neurophysiol. **104**, 1219 (2010).

[4] T. Reichenbach and A. Hudspeth, Rep. Prog. Phys. **77**, 076601 (2014).

[5] G. A. Manley, J. Neurophysiol. **86**, 541 (2001).

[6] P. Martin and A. Hudspeth, Proc. Natl. Acad. Sci. USA **98**, 14386 (2001).

[7] R. Fettiplace and C. Hackney, Nat. Rev. Neurosci. **7**, 19 (2006).

[8] A. Hudspeth, Nat. Rev. Neurosci. **15**, 600 (2014).

[9] P. Martin, D. Bozovic, Y. Choe, and A. Hudspeth, J. Neurosci. **23**, 4533 (2003).

[10] P. Martin and A. Hudspeth, Proc. Natl. Acad. Sci. USA **96**, 14306 (1999).

[11] G. A. Manley and L. Gallo, J. Acoust. Soc. Am. **102**, 1049 (1997).

[12] M. Gelfand, O. Piro, M. O. Magnasco, and A. Hudspeth, PloS ONE **5**, e11116 (2010).

[13] B. Nadrowski, P. Martin, and F. Jülicher, Proc. Natl. Acad. Sci. USA **101**, 12195 (2004).

[14] D. Ramunno-Johnson, C. Strimbu, L. Fredrickson, K. Arisaka, and D. Bozovic, Biophys. J. **96**, 1159 (2009).

[15] Y. Roongthumskul, L. Fredrickson-Hemsing, A. Kao, and D. Bozovic, Biophys. J. **101**, 603 (2011).

[16] J. Howard and A. Hudspeth, Neuron **1**, 189 (1988).

[17] P. Martin, A. Mehta, and A. Hudspeth, Proc. Natl. Acad. Sci. USA **97**, 12026 (2000).

[18] R. Eatock, Annu. Rev. Neurosci. **23**, 285 (2000).

[19] A. Ricci, A. Crawford, and R. Fettiplace, J. Neurosci. **22**, 44 (2002).

[20] R. Fettiplace and A. Ricci, Curr. Opin. Neurobiol. **13**, 446 (2003).

[21] V. M. Eguiluz, M. Ospeck, Y. Choe, A. J. Hudspeth, and M. O. Magnasco, Phys. Rev. Lett. **84**, 5232 (2000).

[22] S. Camalet, T. Duke, F. Jülicher, and J. Prost, Proc. Natl. Acad. Sci. USA **97**, 3183 (2000).

[23] Y. Choe, M. Magnasco, and A. Hudspeth, Proc. Natl. Acad. Sci. USA **95**, 15321 (1998).

[24] J. Tinevez, F. Jülicher, and P. Martin, Biophys. J. **93**, 4053 (2007).

[25] D. Ó. Maoiléidigh, E. M. Nicola, and A. Hudspeth, Proc. Natl. Acad. Sci. USA **109**, 1943 (2012).

[26] J. Barral, K. Dierkes, B. Lindner, F. Jülicher, and P. Martin, Proc. Natl. Acad. Sci. USA **107**, 8079 (2010).

[27] K. Dierkes, B. Lindner, and F. Jülicher, Proc. Natl. Acad. Sci. USA **105**, 18669 (2008).

[28] K. Dierkes, F. Jülicher, and B. Lindner, Eur. Phys. J. E Soft. Matter **35**, 37 (2012).

[29] C. Strimbu, D. Ramunno-Johnson, L. Fredrickson, K. Arisaka, and D. Bozovic, Hearing Res. **256**, 58 (2009).

[30] C. Strimbu, A. Kao, J. Tokuda, D. Ramunno-Johnson, and D. Bozovic, Hearing Res. **265**, 38 (2010).

[31] K.-H. Ahn, J. R. Soc. Interf. **10**, 20130525 (2013).

[32] K.-J. Kim and K.-H. Ahn, Phys. Rev. E **89**, 042703 (2014).

[33] D. Bozovic and A. Hudspeth, Proc. Natl. Acad. Sci. USA **100**, 958 (2003).

[34] D. Ramunno-Johnson, C. E. Strimbu, A. Kao, L. F. Hemsing, and D. Bozovic, Hearing Res. **268**, 163 (2010).

[35] A. W. Peng, T. Effertz, and A. J. Ricci, Neuron **80**, 960 (2013).

[36] A. C. Crawford and R. Fettiplace, J. Physiol. **312**, 377 (1981).

[37] R. Fettiplace, Trends Neurosci. **10**, 421 (1987).

[38] L. Catacuzzeno, B. Fioretti, P. Perin, and F. Franciolini, J. Physiol. **561**, 685 (2004).

[39] F. Jorgensen and A. Kroese, Acta Physiol. Scand. **185**, 271 (2005).

[40] M. Rutherford and W. Roberts, J. Neurosci. **29**, 10025 (2009).

[41] W. Denk and W. W. Webb, Phys. Rev. Lett. **63**, 207 (1989).

[42] A. Hudspeth and R. Lewis, J. Physiol. **400**, 275 (1988).

[43] M. Ospeck, V. M. Eguiluz, and M. O. Magnasco, Biophys. J. **80**, 2597 (2001).

[44] A. B. Neiman, K. Dierkes, B. Lindner, L. Han, and A. L. Shilnikov, J. Math. Neurosci. **1**, 1 (2011).

[45] A. Vilfan and T. Duke, Biophys. J. **85**, 191 (2003).

[46] K. A. Montgomery, M. Silber, and S. A. Solla, Phys. Rev. E **75**, 051924 (2007).

[47] L. Han and A. B. Neiman, Phys. Rev. E. **81**, 041913 (2010).

[48] R. M. Amro and A. B. Neiman, in *International Conference on Theory and Application in Nonlinear Dynamics, Seattle, 2012*, edited by V. In, A. Palacios and P. Longhini (Springer, 2014), p. 237.

[49] T. Holton and A. Hudspeth, J. Physiol. **375**, 195 (1986).

[50] R. Eatock, D. Corey, and A. Hudspeth, J. Neurosci. **7**, 2821 (1987).

[51] E. L. M. Cheung and D. P. Corey, Biophys. J. **90**, 124 (2006).

[52] W. Denk and W. Webb, Hearing Res. **60**, 89 (1992).

[53] D. Clausznitzer, B. Lindner, F. Jülicher, and P. Martin, Phys. Rev. E **77**, 041901 (2008).

[54] I. Bashkirtseva, A. B. Neiman, and L. Ryashko, Phys. Rev. E **87**, 052711 (2013).

[55] Y. Kuznetsov, ftp://ftp.cwi.nl/pub/CONTENT.

[56] P. E. Kloeden and E. Platen, *Numerical Solution of Stochastic Differential Equations*, Vol. 23 (Springer, New York, 1992).

[57] J. S. Bendat and A. G. Piersol, *Random Data Analysis and Measurement Procedures*, 3rd ed. (Wiley, New York, 2000).

[58] A. Pikovsky, M. Rosenblum, and J. Kurths, *Synchronization: A Universal Concept in Nonlinear Sciences*, Vol. 12 (Cambridge University Press, Cambridge, 2003).

[59] A. N. Malakhov, *Fluctuations in Freely Oscillating Systems* (Nauka, Moscow, 1968).

[60] B. Lindner, K. Dierkes, and F. Jülicher, Phys. Rev. Lett. **103**, 250601 (2009).

[61] L. Catacuzzeno, B. Fioretti, and F. Franciolini, J. Neurophysiol. **90**, 3688 (2003).

[62] A. Hudspeth and R. Lewis, J. Physiol. **400**, 237 (1988).